On the Nature of Defects in $Mn_{1-x}Fe_xGe$ Compounds Synthesized under High Pressure

E. G. Iashina[a, b, c, #], E. V. Altynbaev[a, b, c], L. N. Fomicheva[c], A. V. Tsvyashchenko[c], and S. V. Grigoriev[a, b, c]

[a] *Petersburg Nuclear Physics Institute, National Research Center "Kurchatov Institute", Gatchina, 188300 Russia*

[b] *St. Petersburg State University, St. Petersburg, 199034 Russia*

[c] *Institute for High Pressure Physics, Russian Academy of Sciences, Troitsk, 142190 Russia*

[#] *e-mail: iashina_eg@pnpi.nrcki.ru*

Abstract—The mesostructure of $Mn_{1-x}Fe_x$ Ge transition-metal monogermanides is studied by small-angle neutron scattering (SANS) and ultra-SANS in a wide concentration range of $x = 0.0–1.0$.It is shown that the main contribution to the scattering intensity for all concentrations x is made by scattering at crystallites with sharp boundaries and sizes of 1–10 μm, which is described by the squared Lorentzian function. An additional contribution to the scattering intensity as a result of scattering at an ensemble of defects is found as well, which is characteristic of manganese-rich samples. This contribution is well fitted by the power function Q^{-n} with the exponent $n = 3$. The complementary scattering typical of iron-rich samples is described by an exponential function and also seems to be a part of scattering at sharp-boundary crystallites.

Keywords: small-angle neutron scattering, defects, fractal structure, transition-metalmonogermanides, synthesis under high pressure and temperature

INTRODUCTION

One of the main problems in condensed matter physics is searching for correlations between crystal-structure changes and the material characteristics. Real solids always contain defects that form the hierarchical structure which varies upon crystal deformation. These variations can be classified as plastic deformation and defect accumulation. Defect accumulation includes the nucleation, evolution and interaction of defects at different scales of structural levels, as well as the interaction between these levels. The defect density which increases during the course of deformation leads to the emergence of collective properties, such as the establishment of coherent links (correlation) in the defect ensemble, which increases the energy of a system and thus compels it to aim for a relative total energy minimum, forming the dislocation substructures [1]. The establishment of links between defects at the single structure level causes autolocalized formation which serves as the primary structural element at a higher level. Chaotic dislocation structures may lead to tangles, which in turn become oriented cells. There is sometimes a different version of the cascade transition: disoriented cells – strips – substructure with continuous disorientation. The formation of dislocation substructures reflects the signs of the self-organization of dislocation ensembles [2]. The consequence of establishing the hierarchical subordination of structural transitions is the fractal structure of the thermodynamic potential distribution of a dislocation ensemble in configuration space. The fractal structure of a system drastically changes its thermodynamic and kinetic properties. This is due to the division of configuration space into a set of domains with their own statistical ensembles. As a result, the determination of mean values occurs in two stages: averaging is first implemented over the ensemble of a given valley and then over an ensemble of valleys. It is convenient to represent this process as motion within the nodes of the hierarchical Cayley tree, associated with valleys, towards its trunk. Here, the role of time is assigned to plastic deformation [3, 4].

Besides, the consistent description of ensembles of defects and accumulated microcracks, including their spatial organization, is possible only within a fractal concept. The study of multiscale structures, as well as the correlation between them, is difficult, but is possible by small-angle neutron scattering (SANS). SANS is a universal and effective method for solving such issues and is commonly used in condensed-matter physics research areas. Unlike microscopy, techniques based on neutron scattering give structure information about the volume of a sample, which makes them invaluable for studying 3D objects. SANS is one of the most informative tools for studying the structure of matter at the superatomic scales (from units of nano-

meters to tens of microns). Because of the electrical neutrality of neutrons, SANS is a nondestructive and deeply penetrating characterization method that finds wide application in different areas: from the structure of proteins and viruses in biology, medicine and pharmacology to polymer nanocomposites, emulsions and microemulsions in chemistry; from magnetic structures and critical fluctuations at phase transitions in condensed matter physics to the fractal structures of granulated materials in materials science and metallurgy, as well as in mineralogy and geology [5–14].

According to the small-angle neutron scattering concept on a fractal object, the scattering intensity is expressed as a function of the momentum transfer Q:

$$I = \frac{A}{\left(1 + (Q\xi)^2\right)^{n/2}}, \quad (1)$$

where A is the scattering amplitude, ξ is the correlation length of a scattering object and the parameter n describes the fractal properties of the scattering object. At $n = 4$, Eq. (1) is a classic case of scattering from nonfractal 3D inhomogeneities [7, 8], where the scattering object is a biphasic system with randomly distributed particles of different shape with the average size ξ in a homogeneous solution or material. At $4 > n > 3$, Eq. (1) describes scattering from surface fractals forming a particle with a dense nonfractal core surrounded by a fractal layer (fractal surface). At $n \to 3$, the dense core size decreases and the core vanishes at $n = 3$, transforming the surface fractal into a logarithmic fractal. Then, at $3 > n > 2$, the logarithmic fractal transforms into a volume fractal, which, according to classic fractal-geometry vision, corresponds to a self-similar object with a geometric structure repeatable at any scales. The Hausdorff dimensionality of the volume fractal D_H equals to the parameter n from Eq. (1), obtained upon scattering. At $n = 2$, Eq. (1) is a case of scattering at 2D non-fractal objects, or flat particles with the average size ξ.

Here, we present the results of studies of the mesostructure of the $Mn_{1-x}Fe_xGe$ compounds grown under high pressure and temperature by SANS and ultra-SANS methods. It is worth mentioning that, besides structural interest to crystals produced under extreme conditions, attention is also paid to the unique magnetic properties of transition-metal monogermanides with B20 crystallographic structure [11–15]. The helicoidal magnetic order in these compounds is due to the coexistence of strong ferromagnetic interaction and antisymmetric Dzyaloshinskii-Moriya interaction (the Bak–Jensen model [16]), caused by inversion-symmetry violation at atomic positions in the crystal. The spin spiral period varies in them as a function of the transition-metal concentration from tens to hundreds of nanometers [17]. Although the Bak–Jensen model well describes the magnetic properties of FeGe-based compounds [11, 18], the *ab initio* calculations of the MnGe magnetic structure [19, 20] is clearly contrary to the experimental data and thus does not confirm the applicability of the Bak-Jensen model for this type of compounds.

Previously [10], the $Mn_{1-x}Co_xGe$ compound mesostructure was studied by small-angle neutron scattering in a wide concentration range ($x = 0.0$–0.95). The scattering intensity $I(Q)$, obtained for the whole series of samples in the momentum transfer range of 6×10^{-2} nm$^{-1} < Q < 2.5$ nm^{-1}, are described by a power function Q^{-n} with the exponent of $n = 2.99 \pm 0.02$, which gives information on the fractal properties of the sample. This dependence indicates that the ensemble of defects dominant in the superatomic structure is described by the logarithmic spatial correlation function. It is interesting to note that such defects are missing in the isostructural compound FeGe, meaning that the experimental intensity is well fitted by function Q^{-n} with the exponent $n = 4.1 \pm 0.1$. It means that crystallites have a uniform density distribution and a sharp boundary characterizing the surface. As assumed, at ambient pressure, defects in $Mn_{1-x}Co_xGe$ compounds form a logarithmic fractal structure corresponding to a special type of self-similarity with an additive, but not multiplicative (as in the case of a volume fractal [5, 10]) law of scaling.

This work aims at investigating a series of $Mn_{1-x}Fe_xGe$ solid solutions synthesized under pressure by the SANS in the wide momentum transfer range of 10^{-4}–10^{-1} Å^{-1} in order to track the evolution of the morphology of inhomogeneities and defects with varying concentration x. It is shown that, at all concentrations x, the main contribution to the scattering intensity of $Mn_{1-x}Fe_xGe$ systems is made by crystals with sharp boundaries and sizes of 1–10 μm, which is described by the power function $I \sim Q^{-n}$ with the exponent of $n = 4$. Moreover, one can distinguish the contribution made by defect ensembles, which is characterized by the power function Q^{-n} with the exponent of $n = 3$ and associated with a logarithmic spatial correlation function of defects. This scattering is typical for Mn-rich compounds.

SAMPLES AND SYNTHESIS METHODS

$Mn_{1-x}Fe_xGe$ quasi-binary solid solution compounds ($x = 1.0$–0.0, with a step of 0.1) with B20 cubic structure were produced at a pressure of 8 GPa. The high pressure was generated using toroidal cells [21]. Because of the strong differences between the phase diagrams of MnGe and FeGe, [22–24], each of the compounds was synthesized at various temperatures. High temperatures were achieved by indirect heating by means of a NaCl tubular heater with a protective container and a mixture of the initial components inside. The mixture was melted by passing a current through it at a fixed power of melting. After that, the blend was cooled to room temperature with crystalli-

zation of the samples. Finally, the samples were exposed to room-temperature X-ray diffraction (XRD) analysis in order to determine their phase compositions. The synthesis parameters were chosen in accordance with the XRD data by changing the heater power at the same pressure and composition. Synthesis under various conditions was carried out until the XRD results revealed a high impurity content in the sample. Therefore, each compound was exposed to a selected temperature mode to obtain the maximum B20 phase concentration in it. Producing transition-metal monogermanides is a complex task and requires various steps: the synthesis of a sample with a predominant (about 99%)phase content with B20 cubic structure takes 3–5 processing stages.

SMALL-ANGLE NEUTRON SCATTERING EXPERIMENTS FROM $Mn_{1-x}Fe_xGe$ SAMPLES

SANS experiments were carried out on the SANS-1 instrument at the MLZ (Garching, Germany). Measurements were performed at a neutron wavelength of $\lambda = 6$ Å at three detector-sample distances (2.2, 8, and 20 m) and a neutron wavelength of $\lambda = 12$ Å at a detector-sample distance of 20 m. The ultra-SANS experiments were carried out on the KWS-3 instrument at the MLZ at a neutron wavelength of $\lambda = 12$ Å and a detector-sample distance of 10m; the neutron beam was focused by a unique toroidal mirror. The measurements were carried out at room temperature in zero magnetic field on powder $Mn_{1-x}Fe_xGe$ samples (x = 1, 0.8, 0.7, 0.6, 0.5, 0.25, 0.2, 0.1, and 0) placed between two zirconium glasses so that the powder-layer thickness was 0.1 mm. Since the scattering is isotropic, the 2D intensity maps were averaged over the angular component and the 1D scattering intensities were analyzed as a function of the momentum transfer. Figure 1 shows the scattering intensities on a double logarithmic scale for the whole series of $Mn_{1-x}Fe_xGe$ samples. The experimental data are the combined results of SANS and ultra-SANS measurements in the wide momentum transfer range.

Data processing reveals that the scattering intensity is composed of three contributions. The first has to be attributed to scattering at crystallites with a characteristic length ξ, which have a sharp nonfractal boundary. It can be presented by a squared Lorentz function:

$$I_1 = \frac{A}{\left(1 + (Q\xi)^2\right)^2}, \qquad (2)$$

where A is the scattering amplitude and ξ is the correlation length of the scattering object. This contribution is the most significant at all concentrations x. It is worth mentioning that the asymptotic of Eq. (2) at $Q/\xi \ll 1$ is the power function $I_1 \sim Q^{-n}$ with the exponent of $n = 4$, which was previously used for the description of scattering at FeGe mesostructure in the

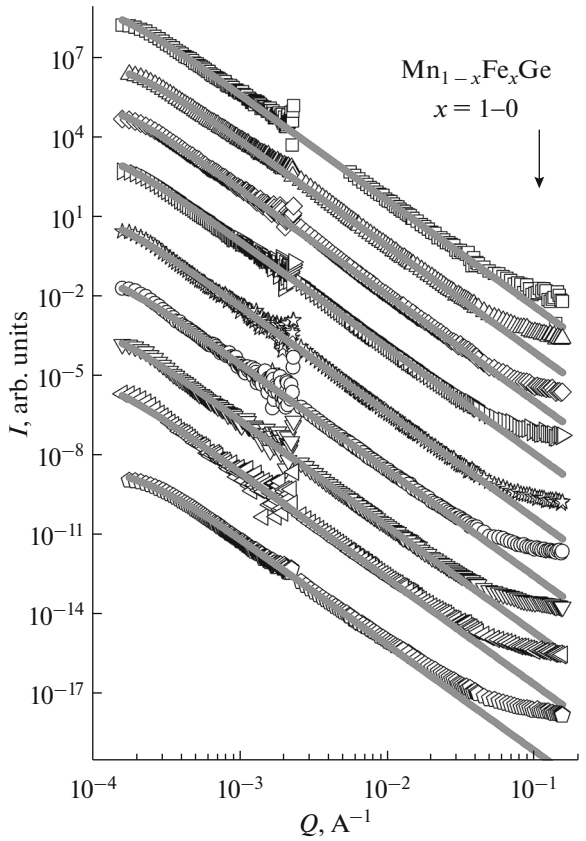

Fig. 1. Scattering intensity as a function of the momentum transfer for $Mn_{1-x}Fe_xGe$ samples (x = 1, 0.8, 0.7, 0.6, 0.5, 0.25, 0.2, 0.1, 0) (open symbols) and relevant approximating curves (gray line) described by Eq. (1).

momentum transfer range of 5×10^{-3}–2×10^{-2} Å^{-1} [10]. The experimental scattering intensities from $Mn_{1-x}Fe_xGe$ compounds were fitted by curves defined by Eq. (2). The parameter ξ as a function of the concentration x is shown in Fig. 2. It should be noted that, in this case, the true value of the parameter ξ is distorted because a direct neutron beam can overlap ultra-small scattering angles. Meanwhile, one can confirm that in all samples of the studied series the crystallite sizes vary from one to several microns.

It should be noted that Eq. (2) does not perfectly describe the experimental data presented in Fig. 1. The additional contribution to the scattering intensity for $Mn_{1-x}Fe_xGe$ mesostructure can be distinguished by subtracting the relevant approximating curve defined by Eq. (2) from the experimental dependence. The difference curves are given in Figs. 3 and 4.

As seen, the difference curve for $Mn_{0.2}Fe_{0.8}Ge$ sample is well described by the sum of two more contributions that are the exponential function in the momentum transfer range of 10^{-3}–10^{-2} Å^{-1} and the cubic function in the momentum transfer range of 10^{-2}–10^{-1} Å^{-1} (Fig. 3). The range limits vary for different

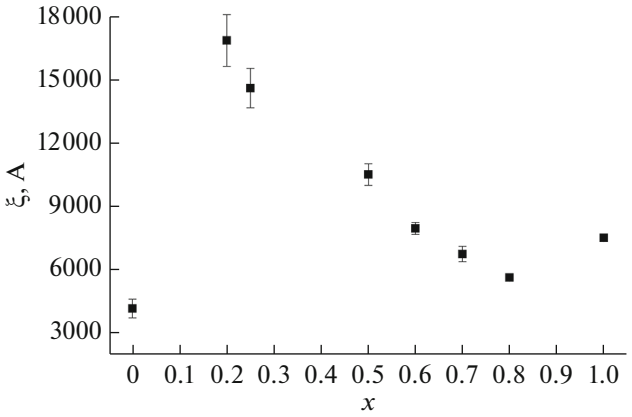

Fig. 2. Parameter ξ as a function of the concentration x in $Mn_{1-x}Fe_xGe$ samples.

values x (see Fig. 4). At higher iron concentrations there is the dominance of the contribution presented by the exponential function

$$I_2 = B\exp(-Q/\delta), \quad (3)$$

whereas, at larger manganese contents, the main contribution is made by scattering obeying the cubic law:

$$I_3 = CQ^{-3} + \text{const}. \quad (4)$$

The difference curve for the $Mn_{0.2}Fe_{0.8}Ge$ sample in Fig. 4 is fitted by the sum of these two functions:

$$I_{2,3} = B\exp\left(-\frac{Q}{\delta}\right) + CQ^{-3} + \text{const}. \quad (5)$$

The smaller the iron concentration, the stronger the cubic contribution in the scattering intensity (Eq. (4)), which reaches a maximum for MnGe (Fig.4). In this case, the cubic contribution to scattering dominates the exponential contribution so much that it is possible to determine the correlation length of the scattering object. Then, the third contribution has to be described by a power function taking into account the finite size of a scatterer:

$$I_{3\text{MnGe}} = \frac{C}{\left(1+(Q\zeta)^2\right)^{3/2}} + \text{const}. \quad (6)$$

Besides, a weak exponential contribution (3) in the momentum transfer range below 2×10^{-3} Å^{-1} is observed. Exponential contribution is perhaps due to crystallites whose shape also impacts the scattering and slightly distorts the squared Lorentz function (Eq. (2)). Therefore, considering that, first, the characteristic contributions described by Eqs. (2) and (3) are close to each other and, second, the form factors have the same physical meaning (the abrupt inhomogeneity boundary), it can be concluded that these contributions come from a single scattering source.

Thus, the analysis of the scattering intensity from $Mn_{1-x}Fe_xGe$ quasi-binary solid solution compounds

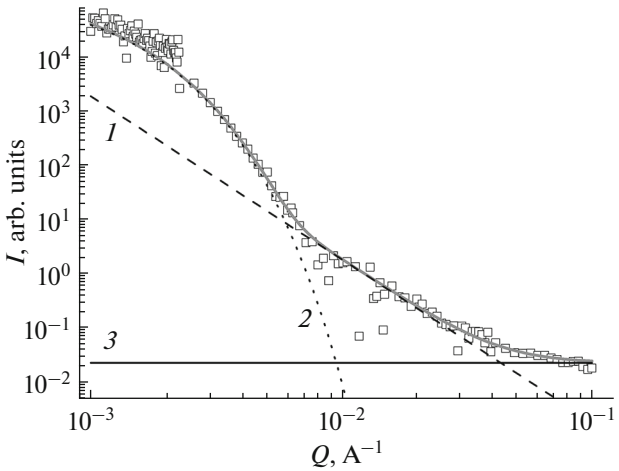

Fig. 3. Difference curve for the $Mn_{0.2}Fe_{0.8}Ge$ sample (open symbols) and relevant approximating curve obtained using Eq. (5) (gray line), which is a sum of the cubic function *1*, the exponential function *2* and the constant describing the background *3*.

indicates that scattering mainly occurs at crystallites with a sharp nonfractal boundary and sizes of several microns. Moreover, crystallites have a defect structure, and scattering from it is described by the cubic law in reciprocal space, which corresponds the logarithmic fractal structure of defects ensemble [5, 9, 10]. The amplitude of cubic contribution increases as the manganese content increases. In the case of pure MnGe, in addition to the fractal organization of the defects ensemble, the correlation length is found to be $\zeta = 210 \pm 10$ Å^{-1}.

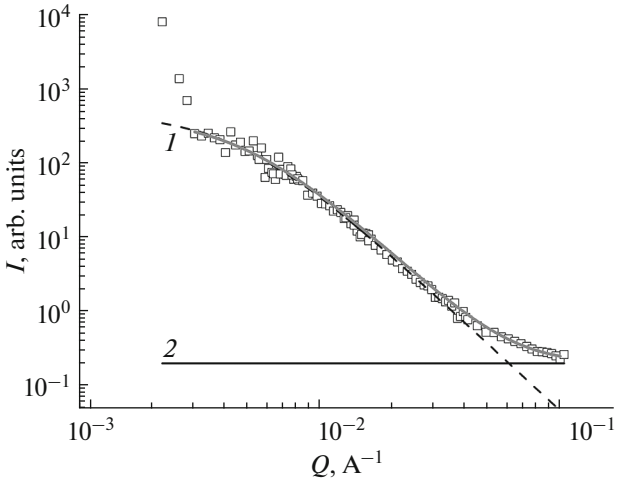

Fig. 4. Difference curve for the MnGe sample (open symbols) and relevant approximating curve obtained using Eq. (6) (gray line), which is a sum of the cubic function taking into account the finite size of scatterer Eq. (6) *1* and a constant describing the background *2*.

CONCLUSIONS

A $Mn_{1-x}Fe_xGe$ transition-metal monogermanide mesostructure at concentrations of $x = 1.0–0.0$ was studied by small-angle neutron scattering in the momentum transfer range of $[2 \times 10^{-4}–2 \times 10^{-1}]$ Å^{-1}. Scattering of two types was found. Scattering from crystallites is characterized by the sum of the squared Lorentz function and a exponential function whereas scattering from the ensemble of defects is described by a cubic law. We mention that the law $Q^{-3}$is also typical of scattering from defects that are present in $Mn_{1-x}Fe_xGe$ compounds [10]. It is apparent that the logarithmic fractal structure is characteristic of an ensemble of defects arising in the course of the cooling of crystals stabilized under high pressure.

ACKNOWLEDGMENTS

We are grateful to B. Wu and A. Heinemann, responsible for the KWS-3 and SANS-1 neutron stations, for help in taking the measurements.

FUNDING

This work was supported by the Russian Science Foundation, project no. 17-12-01050.

REFERENCES

1. N. Hansen and D. Kuhlman-Wilsdorf, Mater. Sci. Eng. **81**, 38 (1986).
2. O. B. Naimark, Fiz. Mezomekh. **6** (4), 45 (2003).
3. A. I. Olemskoi and A. Ya. Flat, Phys. Usp. **36**, 1005 (1993).
4. A. I. Olemskoi and I. A. Sklyar, Sov. Phys. Usp. **35**, 455 (1992).
5. E. G. Iashina, E. V. Velichko, M. V. Filatov, W. G. Bouwman, C. P. Duif, A. Brulet, and S. V. Grigoriev, Phys. Rev. E **96**, 1 (2017).
6. A. Munoz, M. A. Monge, B. Savoini, R. Pareja, and A. Radulescu, Int. J. Refract. Met. Hard. Mater. **61**, 173 (2016).
7. J. Bahadur, Y. B. Melnichenko, L. He, C. I. Contescu, N. C. Gallego, and J. R. Carmichael, Carbon **95**, 535 (2015).
8. R. Yang, Sh. He, O. Hu, M. Sun, D. Hu, and J. Yi, Fuel **197**, 91 (2017).
9. E. G. Iashina and S. V. Grigoriev, J. Surf. Invest.: X-ray, Synchrotron Neutron Tech. **11**, 897 (2017).
10. I. A. Safiulina, E. V. Altynbaev, E. G. Iashina, A. Heinemann, L. N. Fomicheva, A. V. Tsvyashchenko, and S. V. Grigoriev, Phys. Solid State **60** (4), 751 (2018).
11. E. Altynbaev, S.-A. Siegfried, V. Dyadkin, E. Moskvin, D. Menzel, A. Heinemann, C. Dewhurst, L. Fomicheva, A. Tsvyashchenko, and S. Grigoriev, Phys. Rev. B **90**, 174420 (2014).
12. E. V. Altynbaev, A. S. Sukhanov, S.-A. Siegfried, V. A. Dyadkin, E. V. Moskvin, D. Menzel, A. Heinemann, A. Schrayer, L. N. Fomicheva, A. V. Tsvyashchenko, and S. V. Grigoriev, J. Surf. Invest.: X-Ray, Synchrotron Neutron Tech. **10**, 777 (2016).
13. N. Martin, M. Deutsch, F. Bert, D. Andreica, A. Amato, P. Boni, R. de Renzi, U. K. Rossler, P. Bonville, L. N. Fomicheva, A. V. Tsvyashchenko, and I. Mirebeau, Phys. Rev. B **93**, 174405 (2016).
14. E. Altynbaev, S.-A. Siegfried, E. Moskvin, D. Menzel, C. Dewhurst, A. Heinemann, A. Feoktystov, L. Fomicheva, A. Tsvyashchenko, and S. Grigoriev, Phys. Rev. B **94**, 174403 (2016).
15. B. Lebech, J. Bernhard, and T. Freltoft, J. Phys.: Condens. Matter **1**, 6105 (1989).
16. P. Bak and M. H. Jensen, J. Phys. C **13**, L881 (1980).
17. S. V. Grigoriev, N. M. Potapova, S.-A. Siegfried, V. A. Dyadkin, E. V. Moskvin, V. Dmitriev, D. Menzel, C. D. Dewhurst, D. Chernyshov, R. A. Sadykov, L. N. Fomicheva, and A. V. Tsvyashchenko, Phys. Rev. Lett. **110**, 207201 (2013).
18. S. V. Grigoriev, S. V. Maleyev, A. I. Okorokov, Y. O. Chetverikov, P. Boni, R. Georgii, and K. Pranzas, Phys. Rev. B **74** (21), 214414 (2006).
19. T. Koretsune, N. Nagaosa, and R. Arita, Sci. Rep. **5**, 13302 (2015).
20. J. Gayles, F. Freimuth, T. Schena, G. Lani, P. Mavropoulos, R. Duine, S. Blugel, J. Sinova, and Y. Mokrousov, Phys. Rev. Lett. **115**, 036602 (2015).
21. L. G. Khvostantsev, V. N. Slesarev, and V. V. Brazhkin, High Press. Res. **24**, 371 (2004).
22. E. Arras, D. Caliste, T. Deutsch, F. Lancon, and P. Pochet, Phys. Rev. B **83** (17), 174103 (2011).
23. E. I. Tonkov, *High Pressure Phase Transformations, A Handbook* (CRC, Boca Raton, FL, 1992).
24. Y. H. Zhuang, X. Chen, J. L. Yan, R. F. Li, C. H. Ma, J. Alloys Compd. **465** (1), 216 (2008).